Energy loss of keV fluorine ions scattered off a missing-row reconstructed Au(110) surface under grazing incidence

L. Chen,[1,2] J. Shen,[1] J. E. Valdés,[3] P. Vargas,[3] and V. A. Esaulov[1,*]

[1]*Institut des Sciences Moléculaires (Unité Mixte de Recherche CNRS Université, UMR 8214), bât 351, Université de Paris Sud, Orsay F-91405, France*

[2]*School of Nuclear Science and Technology, Lanzhou University, Lanzhou 730000, China*

[3]*Department of Physics, Universidad Técnica Federico Santa María, Valparaíso, Casilla 110-V, Chile*

(Received 1 October 2010; published 2 March 2011)

A joint experimental and theoretical study of energy loss is presented for 1-to-4-keV fluorine negative ions in grazing scattering on a missing-row reconstructed Au(110) surface. Measurements of energy losses for various azimuthal orientations of the crystal have been performed by means of a time-of-flight method with a pulsed beam. The dependence of the fraction of surviving negative ions on azimuthal angles, was determined. Our energy-loss data are discussed in light of trajectory and stopping-power calculations, where the explicit inclusion of the nonuniform electron density at the surface provides good agreement with the experimental data. The simulation allows us to delineate various trajectory classes that correspond to different contributions in the energy-loss spectra for various azimuthal orientations of the surface.

DOI: 10.1103/PhysRevA.83.032901 PACS number(s): 34.50.Bw, 79.20.Rf

I. INTRODUCTION

Energy-loss phenomena of energetic ions in matter have attracted much attention because of their importance in fundamental research as well as in technological applications as an analytical tool. In the low-velocity regime ($v \leqslant v_0 =$ bohr velocity), particles lose energy when they interact with matter due to elastic loss (that is, collisions with screened nuclei without any excitation) and inelastic loss (that is, electronic energy loss via electron-hole pair generation). Both energy-loss mechanisms compete depending on impact parameter and particle mass. For collisions in surface grazing scattering and in channeling conditions [1–3], projectiles collide in a sequence of correlated small-angle or large-impact-parameter events. As opposed to small-impact-parameter collisions, where inner shell excitations can occur leading to large energy losses in a single binary encounter [4], here energy losses in individual encounters remain small. Also in this case the elastic loss does not make an important contribution to the total particle energy loss. This condition is easily met by the steering of the projectile between neighboring atomic strings (axial surface channeling) or planes (semiplanar surface channeling). Both channeling phenomena occur when the projectile is scattered from a surface in grazing incidence, with angles less than the Lindhard critical angle [5]. In the surface channeling regime, the energy transfer of the projectile to lattice atoms of the crystal is very small because of large impact parameters so that electronic energy-loss phenomena can be directly investigated [5–7].

The description of ion slowing down during channeling in crystals and grazing scattering on surfaces is complicated because of inhomogeneity in the electronic density. In transmission experiments, electronic ion energy loss is greatly reduced in channeling orientations compared to that seen with a random orientation [8]. The case of ion-surface scattering is particularly complex because regions far from the first atomic layer, where the electronic density decreases, contribute to energy losses. The trajectory lengths depend on the scattering conditions, such as incident and azimuthal angles, and one must correctly account for the spatial inhomogeneity, or corrugation, of the electron density in the crystal and above the surface. Several recent experimental and theoretical investigations have focused on these problems [5,6,9–18], but in these, an averaged electron density for a given distance from the surface is assumed, which is a poor description of the electron density corrugation above a crystal, especially in high-symmetry directions. Thus, for instance, we found it impossible [18] to fit our data for energy losses on Ag(110) over an extended energy range because very different trajectory types are found. However, we have recently developed an approach to describe slowing of ions through solids under conditions of strongly varying electron densities. We have applied it to the case of proton scattering through crystals [19] and in scattering on the Ag(110) surface [20].

In this paper, we report the main features of an experimental and theoretical study of the energy losses of low-energy fluorine ions scattered under grazing incidence on a Au(110) surface for various crystalline directions. We chose fluorine, because energy losses of slow heavy ions have not been the object of very detailed investigations as opposed to light-ion scattering. The Au(110) surface was chosen because it displays a missing-row reconstruction and is thus highly corrugated. Taking correctly *into account the inhomogeneity of the surface electronic density seemed essential*. This case thus provides a good testing ground for our model. Our experiments indeed showed very strong variations in the characteristics of energy losses when scattering along different azimuthal directions along the surface, where the ions encounter very different electron density contours. Our approach allows us to account for these variations and we are thus able to analyze these energy losses in terms of the ion trajectories and the electron densities encountered. A very brief preliminary account of some results for 4 keV was presented elsewhere [21], along with a description of the theoretical approach we use.

*Corresponding author: vladimir.esaulov@u-psud.fr

In scattering of ions on surfaces, Auger and resonant electron transfer processes play an important role [22–24]. In the grazing scattering of fluorine ions on a surface, resonant electron loss and capture phenomena take place [23,24]. These involve transitions of an electron between the valence band and the anion level of the scattered particle, the latter being shifted down due to image potential effects [5]. Though this is not the main objective of this work, we obtained some information on resonant electron transfer and in particular the dependence of the survival negative-ion fraction on azimuthal angles.

The experiments and the simulation model are described in the next sections. We use atomic units throughout this paper, unless otherwise specified.

II. EXPERIMENT

We performed a time-of-flight (TOF) study in order to measure the energy loss of keV fluorine atoms and ions after grazing scattering on the surface. The experimental setup of our TOF studies is sketched in Fig. 1(a). Briefly, fluorine negative ions are produced in a discharge source using CF_4 mixed with Ar. The ions are mass selected and deflected through 10° to eliminate photons and neutrals and then pass first through sets of defining slits and a chopping system consisting of a pair of electric-field plates before entering into the main ultrahigh-vacuum (UHV) chamber.

Measurements were made for specular scattering conditions with an incident angle of 3.5° as measured with respect to the surface plane, that is, through a total scattering angle of 7°. The scattered particles are recorded by a position-sensitive 34-mm-diameter channel plate detector set at a distance of 1.98 m from the scattering center at the end of a TOF analysis tube. This detector is equipped with three discrete anodes so that the incoming positive and negative ions and neutrals can be separated using a deflector plate assembly and thus be detected simultaneously by each of the anodes [see Fig. 1(a)]. The detecting system has an acceptance angle of about 0.08° in the scattering plane and 0.2° in the out-of-plane direction. The incident beam maximum divergence as defined by collimation slits is ±0.25° in the scattering plane.

TOF spectra were recorded for various azimuthal angular settings for every charge state. We only discuss TOF spectra for scattered neutrals throughout this paper unless otherwise specified because of efficient neutralization after impinging the surface. The energy losses are determined with respect to the energy of the incident electrically reflected beam. This corresponds to scattering with a repulsive voltage applied to the sample so that the ions do not undergo any inelastic processes.

The Au(110) sample was bought polished to 0.05 μm. *In situ* preparation consisted of repeated cycles of small grazing incident angle (a few degrees, usually less than 3.5°), sputtering with 4 keV Ar^+ ions, and annealing to 720 K for about 10 min. After following the careful preparation procedure detailed in Refs. [25,26], a (1×2) missing-row reconstructed surface was obtained. The characteristics of the scattered beam profile (see below) confirm this. During sputtering, the crystal was rotated azimuthally in order to avoid induction of structures due to sputtering. The azimuthal angle α is defined as an angle in the surface plane relative to a given Miller-index crystallographic direction as shown

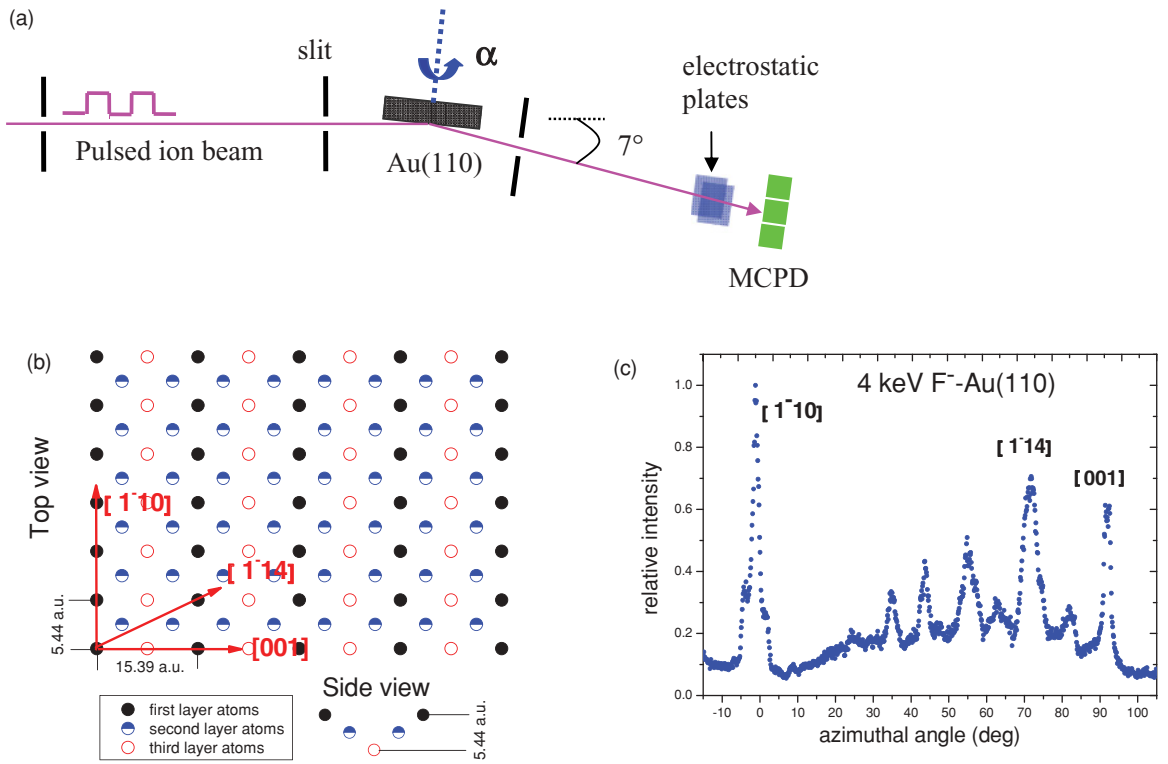

FIG. 1. (Color online) (a) Schematic diagram of the experimental setup. Shown is the TOF line after scattering off the surface of the target. (b) Schematic diagram of the (1×2)-Au(110) surface and the azimuthal angle nomenclature used in the paper. (c) An azimuthal scan of 4-keV fluorine ions in grazing scattering on the surface.

in Fig. 1(a). The chamber pressure during measurements was typically 5×10^{-8} Pa.

The crystal azimuthal setting is determined by measuring the scattered intensity of the ion beam in the forward direction during an azimuthal scan. This allows a precision better than 0.2°. Figure 1(b) shows the schematic diagram of the (1×2)-Au(110) surface and the angle nomenclature used in the paper, that is, the azimuthal angle is termed 0°, when it corresponds to the crystal direction $[1\bar{1}0]$ and has negative values when rotating the red arrow counterclockwise. Figure 1(c) shows a typical azimuthal scan, for scattering of 4-keV F^-ions in specular reflection geometry when both F^0 and F^- are detected. The structures in the spectrum correspond to the crystal directions indicated in Fig. 1(b), that is, azimuthal angles of 70.5° and 90° correspond to the crystal directions of $[1\bar{1}4]$ and [001], respectively. These well-defined structures in the spectrum also indicate the high quality of the surface after the preparation procedure.

III. RESULTS

A. Ion fractions

In our experiments the neutrals and ions are recorded simultaneously and separately using our continuous beam mode. We are thus able to determine electron-transfer probabilities or survival ion fractions. We find that almost all negative fluorine ions are neutralized at a grazing incident angle (3.5°). The ion fraction is around 0.6%–1.3%, as shown in Fig. 2. An interesting feature here is that we observe a significant azimuth-dependent variation of the ion fraction, which has not been reported previously on metal surfaces. It is found that a minimum appears at 0°, corresponding to scattering between the added rows for 4-keV and 3-keV incident ions. Measurements were not performed at lower energies because of the small values of the ion fraction.

In some of our past work ([22–24]), the negative-ion fraction was determined for various values of a surface work function (ϕ). The negative-ion fraction of F^- ions scattering on Ag ($\phi = 4.3$ eV) is about 50% for 4-keV F^- ions [23].

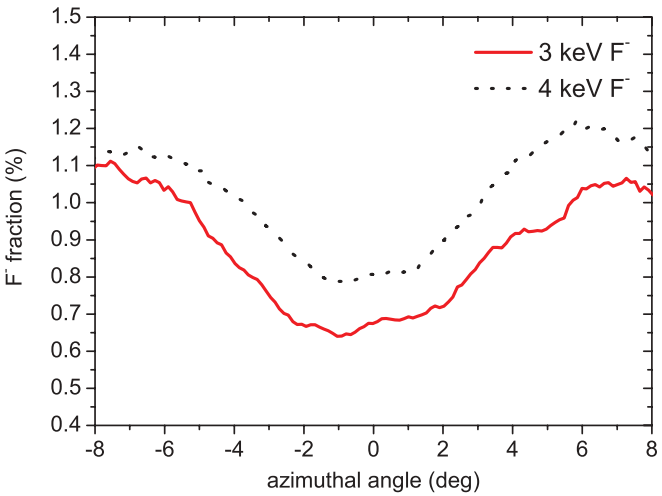

FIG. 2. (Color online) Survival negative fractions of 3-keV and 4-keV F^- ions scattered off a Au(110) surface as a function of the azimuthal angle.

For the case of a surface with a work-function value closer to that of gold, that is, Pd(100), with a value of ϕ about 5 eV, we found [27] an ion fraction value of about 9% for a somewhat lower 500-eV energy. In those measurements, this was not determined for higher energies. From general considerations on resonant electron transfer it seems reasonable to expect a smaller value of the negative-ion fraction for higher-work-function surfaces such as Au(110) ($\phi = 5.4$ eV). We do not make attempts to model the measured behavior of the fraction, since we believe this would require a complicated description involving both trajectory analysis and a proper inclusion of the corrugation of the surface in the description of electron capture and loss processes. This is not the emphasis of this paper, focused on the slowing down of the projectile. It is plausible that this effect is related to the strong corrugation of the electron density above the surface leading to rather different "effective" atom-surface interaction distances akin to the effect of scattering on a stepped surface.

B. Energy losses

Figures 3 and 4 show the evolution of the energy losses of 1-to 4-keV F^- ions as a function of some azimuthal orientations of the Au(110) surface. Rather strong changes are observed for scattering along different crystal orientations. These are summarized in Fig. 3. The most obvious difference is the clearly defined double peak structure that appears for the 70.5° direction and the 3.6° for some incident energies.

A more detailed evolution of these energy losses is shown in Fig. 4. One can see that near the 0°, 90°, and 70.5° directions rapid changes occur and the double-peaked structures appear and disappear over a narrow azimuthal angular range.

In Fig. 5(a), we present the most probable energy loss (corresponding to the peak maximum) for some incident energies and azimuthal angles around the 0° direction. It should be noted that we chose the most probable energy loss corresponding to the lower energy-loss peak, when a double-peak structure appears around 0°. The relative variation of energy loss is about 40%–75% in the vicinity of 0°, with respect to a "random" direction. In Fig. 5(b), showing the most probable energy losses, we observe that these are found to increase linearly with the increase of incident energies. The energy loss is the smallest for a random orientation (here 29.7°) of the target and is larger for the other orientations.

IV. ENERGY-LOSS MODEL AND PARTICLE-TRAJECTORY SIMULATIONS

We now present results of our simulations of the energy-loss spectra. Our aim here is to understand the characteristics of the energy-loss spectra shown above, in terms of trajectories of scattered neutrals and the encountered electron-density regions. We aim in particular to understand the origin of the double-peak structures observed. We use a deterministic semiclassical approach, specifically developed for the study of the energy-loss dependence with the particle trajectory and the particle charge state. This model has been applied to other situations, where the agreement with measured data for scattering on Ag(110) was good [20]. Here we give

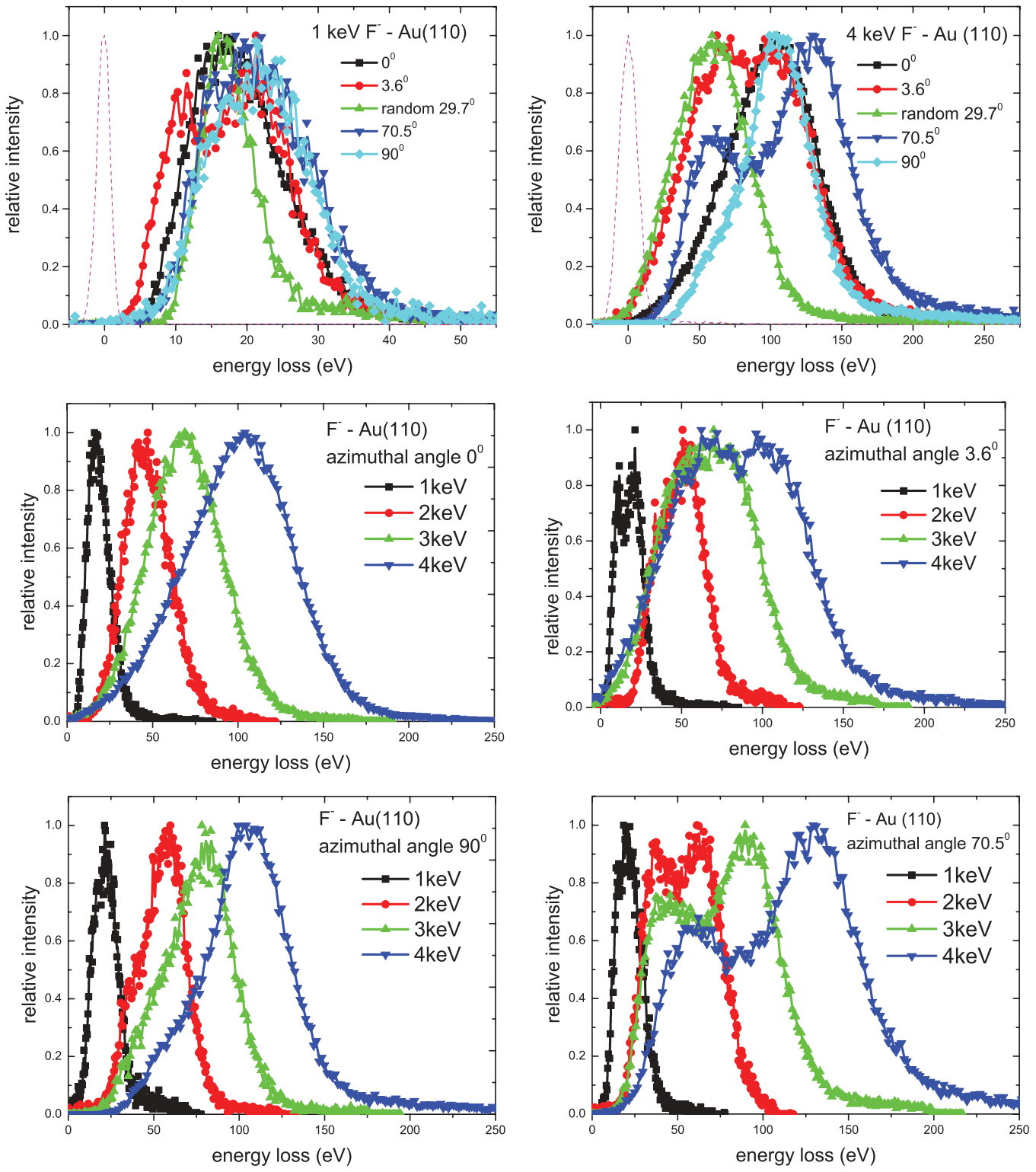

FIG. 3. (Color online) Energy-loss spectra of 1-to-4-keV F^- ions scattered off a Au(110) surface for different azimuthal angles. The incident beam profile (dashed line) is shown for 1- and 4-keV fluorine ions.

a brief description of how this approach is applied to a fluorine-gold interaction. A more complete description of these simulations is given in our recent work [20,21] and references therein.

Particle trajectories in solids are determined using the Newton's equation [see Eq. (1)] which contains:

(1) the repulsive interaction force between the particle and lattice atoms (through interatomic screened potentials);

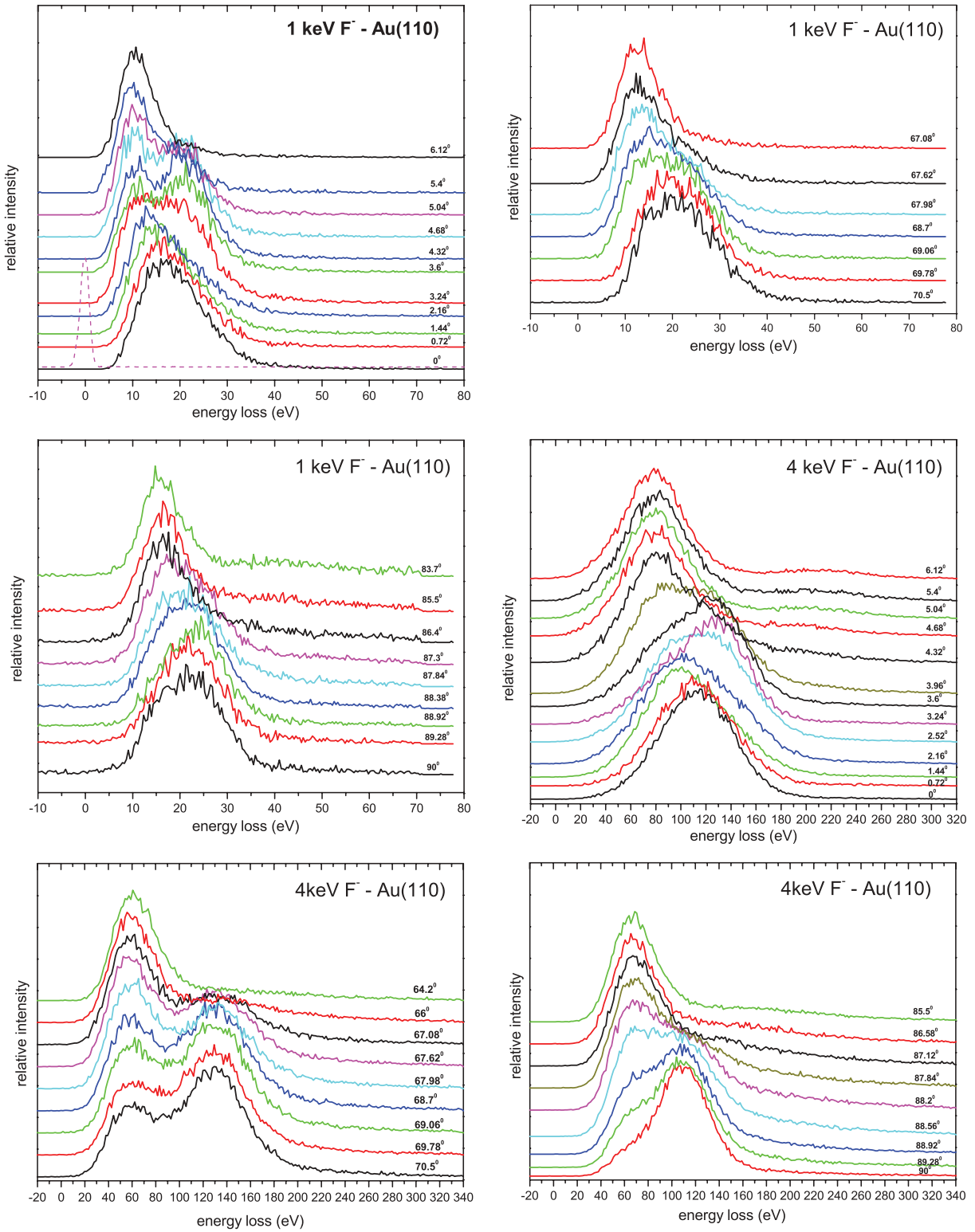

FIG. 4. (Color online) The evolution of the energy-loss spectra measured for different azimuthal angles (around 0°, 70.5°, and 90°, respectively) for 1- and 4-keV F^- ions scattered off a Au(110) surface. The incident beam profile (dashed line) is shown for 1-keV fluorine ions.

(2) the stopping force due to the particle interaction with valence electrons, via the electron-hole pair excitation that depends on the particle velocity and the spatial electron density; and

(3) the image force interaction due to the polarizing effect of the charged particle on the electron distribution of first atomic layers depending on the particle position above the surface.

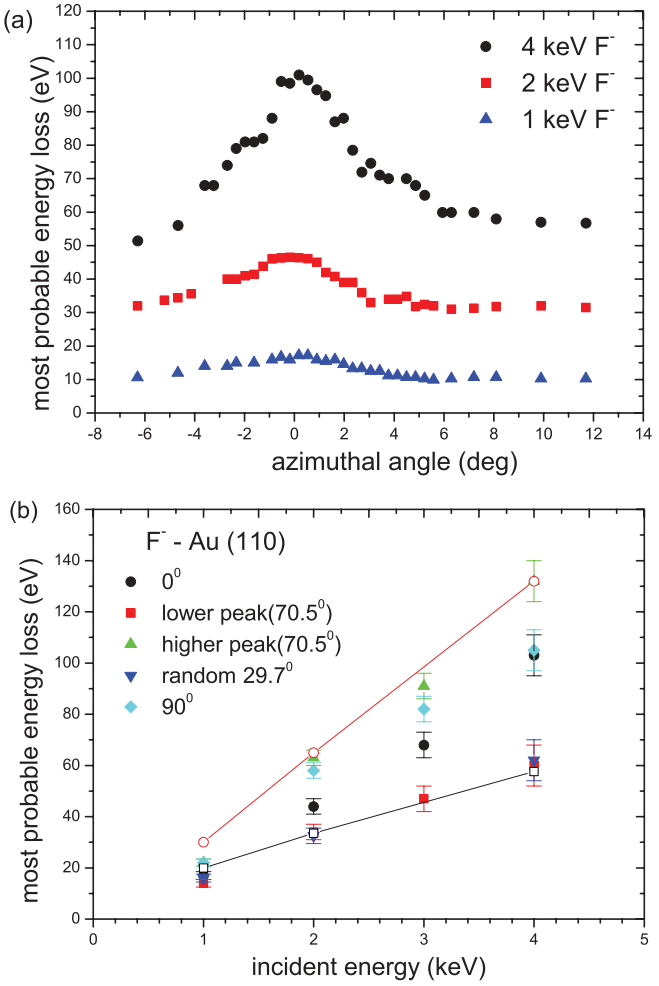

FIG. 5. (Color online) (a) Azimuthal angle dependence of the most probable energy loss of 1-keV, 2-keV, and 4-keV F^- ions scattered from a Au(110) surface around 0°. (b) The most probable energy loss of F^- ions scattered from a Au(110) surface as a function of incident energies for different azimuthal angles. As shown in Figs. 3 and 4, a double-peak structure of the energy-loss spectra appears for the 70.5° azimuthal angle, where the most probable energy loss (■) corresponds to the lower energy-loss peak and (▲) to the higher energy-loss peak. Also shown are the calculated results for the 70.5° azimuthal angle: the lower energy-loss peak (□) and the higher energy-loss peak (○). The lines through the data guide the eye.

Then the Newton equation can be written as

$$\vec{F}(\vec{r}) = M\frac{d^2\vec{r}}{dt^2} = M[-\nabla V_l(\vec{r},\vec{R}) - \nabla V_i(z) + \vec{f}(\vec{v},n(\vec{r}))]. \quad (1)$$

Here z is the particle surface distance as measured from the first atomic layer. Negative values of z will refer to distances above the surface. M is the projectile mass. In our calculations the interaction potential between the projectile, Z_1, and the target atoms, Z_2, is assumed to be of the Lenz-Jensen [28] type, with a Thomas-Fermi screening length given by

$$a_{TF} = \left[\frac{9\pi^2}{128}\right]^{1/3}\left(Z_1^{1/2} + Z_2^{1/2}\right)^{-2/3}. \quad (2)$$

This potential was used because in a previous work we compared different interatomic potentials for the case of the H^+ scattering on Ag(110) [20] and concluded that this approach describes very well the shapes of energy-loss distributions, which depends on the particle trajectories that are driven by the interatomic potential. We adjust slightly the screening length to achieve the best fitting for energy-loss distributions. For this procedure we follow the study of O'Connor and Bierzack [29] about the use of empirical interatomic potentials.

The force on the projectile induced by the image charge is modeled by the image potential in the approximation of Jones *et al.* [30], in atomic units, and is given by

$$V_{\text{imag}}(z) = \begin{cases} \frac{1}{4(z-z_0)}\{1 - e^{-\lambda(z-zo)}\}, & z < z_0 \quad \alpha = \frac{2U_0}{\lambda} - 1 \\ \frac{-U_0}{\alpha e^{-\beta(z-zo)}+1}, \text{ otherwise} & \beta = \frac{U_0}{\alpha} \end{cases}. \quad (3)$$

This analytic form was used because it is a close approximation of the results for jellium and density functional calculations of the barrier potential. Parameters corresponding to a Au(110) surface are $z_0 = -1.86$ a.u., $U_0 = 0.605$ a.u., $\lambda = 0.9$ a.u. [31]. In our model calculations we use these parameters for the image force; that is, we consider a flat image plane position. In fluorine scattering electron transfer occurs and we include it semiempirically as described in Ref. [21].

The last term in the Newton equation gives the "frictionlike" force that models the particle energy loss due to the energy transfer to the valence electrons. This is calculated in a continuous slowing-down process during its trajectory. This force is proportional to the ion velocity and has a nonlinear dependence on the local electron density $n(\vec{r})$. Additionally, we introduce the energy loss straggling in order to take into account the stochastic character of the collisions between ions and electrons. This parameter will give the broadening in the energy-loss distribution and is also proportional to the ion velocity. Its dependence on the local electron density is nonlinear. In our simulations this parameter is taken into account in a stochastic way where, following a normal random distribution for the energy loss straggling in each time step of the particle trajectory; that is, we add or subtract a random amount of energy to the instantaneous energy of the particle according to the local electron density (see [21]).

For a given electron density the ion energy loss is proportional to the ion velocity and for each time step the energy loss is calculated using the local density approximation (LDA). Both energy-loss parameters are obtained by solving Schrödinger's equation for the scattering of electrons by a known hydrogeniclike screened potential or a self-consistent potential obtained using the density-functional formalism (DFT) and the transport cross-section (TCS) approach [21].

An essential ingredient in the calculations is the electron density that describes the electronic structure of the material besides the atomic crystal structure. The inhomogeneous spatial electron density distribution is obtained through first-principles density-functional theory using the *ab initio* linear muffin-tin orbitals (LMTOs) within the LDA. As remarked in Ref. [21], we use the spatial electron density distribution in order to obtain a more accurate description of the electronic energy-loss processes for particles interacting with solid matter and to explain the energy loss as a function of the azimuthal

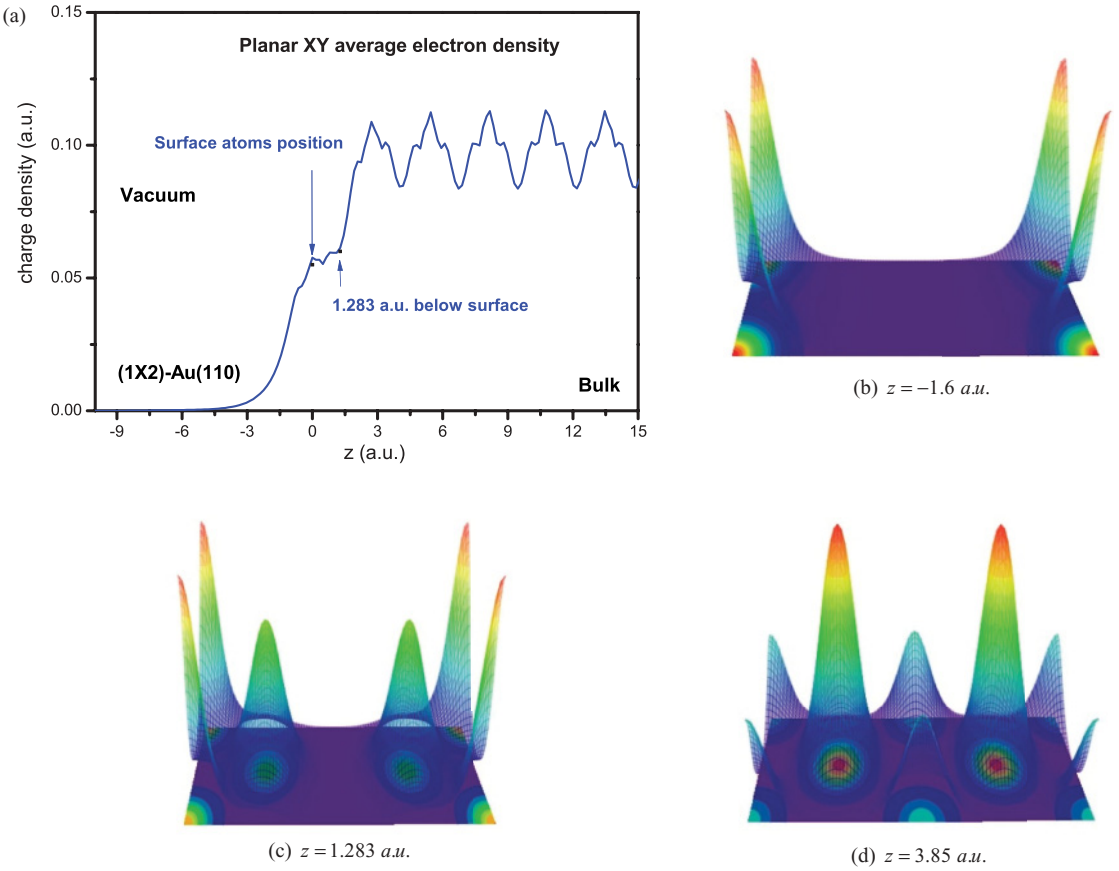

FIG. 6. (Color online) (a) Planar average (*XY*) charge density profile for a reconstructed Au(110) surface as a function of depth z; (b)–(d) Spatial charge density profiles at distances $z = -1.6$ a.u. above the first atomic layer, $z = 1.283$ a.u. below the first layer and $z = 3.85$ a.u. below the second layer of the surface, respectively. All of these density profiles are given along the $[1\bar{1}0]$ or 0° direction [see Fig. 1(b)]. The color map density profile stretches from low density (indigo) to high density (red). Numerical values for the density for these limits are the following: (b) 0.0013–0.1692 a.u.; (c) 0.0031–0.3524 a.u., (d) 0.024–0.4275 a.u.

angle. In Fig. 6(a) we show the planar average (*XY*) of the electron density for the Au(110) (1×2) missing-row surface. Here we define the z axis as perpendicular to the surface plane. In Figs. 6(b)–6(d) we show the spatial charge density for different values of the z position for the $[1\bar{1}0]$ direction [for reference see Fig. 1(b)]. In this figure the values are "special" and are related to trajectory types that we discuss below.

V. DISCUSSION

In the following we attempt to analyze the characteristics of the energy-loss spectra on the basis of the model described in Sec. IV above. We try to delineate some of the main features of heavy ions scattering in terms of their trajectories and encounter regions of different electron densities leading to different energy losses.

Because the simulations require very lengthy calculations, involving hundreds of thousands of trajectories, we limit ourselves here to some special cases, where the energy-loss spectra have very distinctive features. Here we present spectra for 1 and 4 keV for the 0° and 90° directions, where energy losses are large and also spectra for 1, 2, and 4 keV for the 70.5° direction, where we observe a splitting of the energy-loss spectrum into two components. Calculated spectra are shown in Fig. 7. As can be seen, the overall features and magnitude of the energy losses are correctly reproduced, though sometimes some minor imperfections remain such as the longer tails observed in some spectra.

In order to analyze the features of the long-tailed spectrum for 0° azimuth, we show in Fig. 8 a side view of the Au(110) surface in which the points indicate the apex position of the ion trajectories, which actually reach the detector (see Fig. 1, for definition of directions) for the case of 4-keV fluorine ion scattering in the 0° and 70.5° directions.

For 0° we have subdivided the zones into categories (1, 2, and 3) corresponding to particles that stay above the first layer, the second layer, and the third layer. The electron densities "seen" by the projectile for these "special" distances above and below the surface are shown in Fig. 6.

The corresponding contributions to the full spectrum are also shown in Fig. 7. As could be intuitively expected, the energy losses increase when going deeper into the surface. The overall shape of the spectrum is determined by the relative weight of the different trajectories.

In the case of the 90° direction, the slight hump on the low-energy-loss side comes from trajectories on top of the surface. The dominant contribution to the ion energy loss comes from trajectories below the surface.

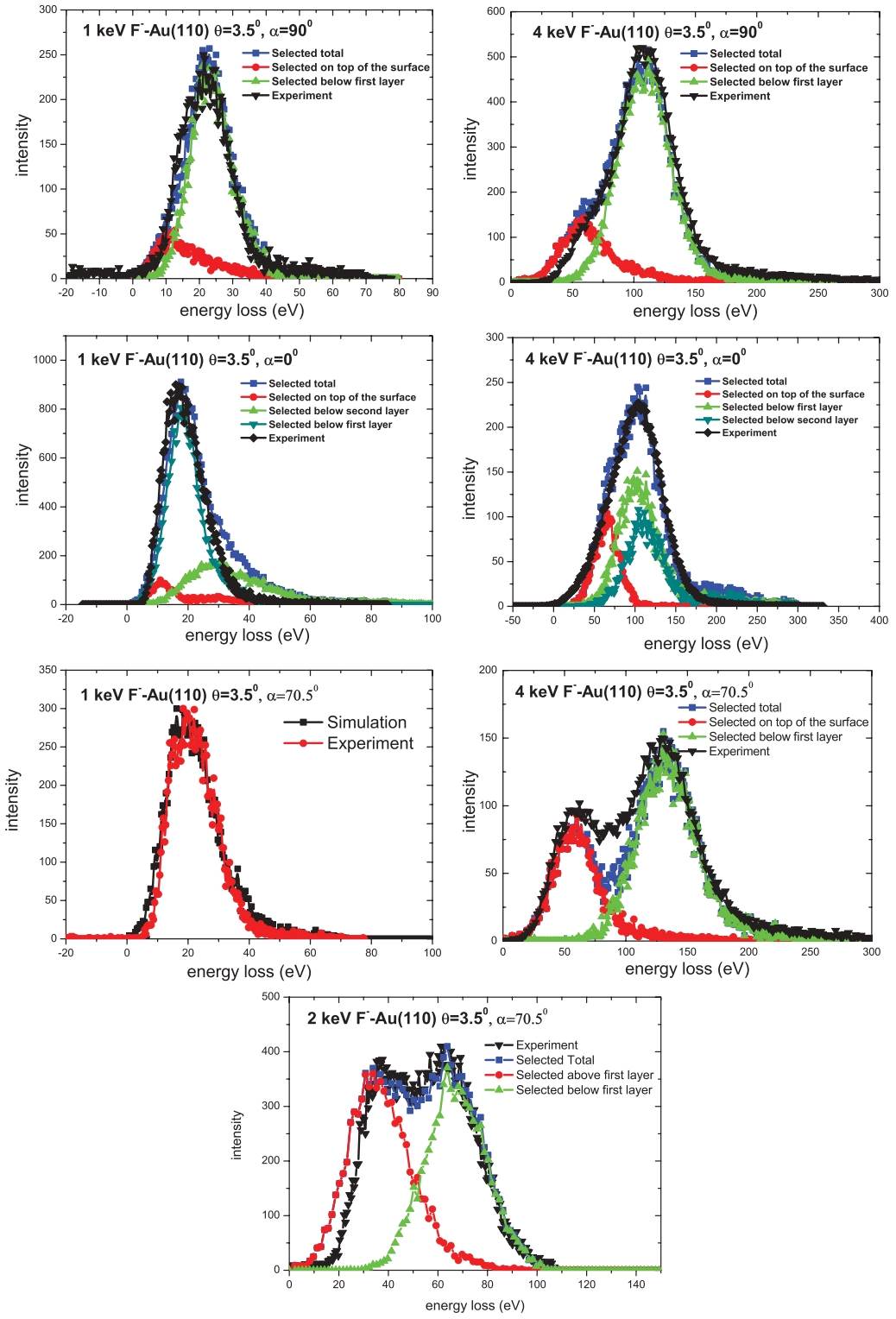

FIG. 7. (Color online) Simulated energy-loss spectra for 1-keV, 2-keV, and 4-keV F^- scattered along different azimuthal angles for Au(110). The different subcomponents of the simulated spectra, representing the different energy losses, correspond to particles coming from different impact zones probed by the ion in the above-surface and subsurface regions as shown in Fig. 8. The spectrum marked with "selected total" is the sum of the different subcomponents of the simulated spectra. In the plots experimental spectra are also shown.

The contributions of these two types of trajectories are more obvious for 70.5°. Indeed, the reason for the splitting of the energy-loss peak for the 70.5° direction is due to groups of trajectories [see Fig. 8(b)] that correspond to scattering mainly on top of atomic rows, which lead to lower energy losses and to trajectories that penetrate more into the solid and result in larger energy losses, because these explore regions of higher electron densities. This is illustrated in Fig. 9, where we plot

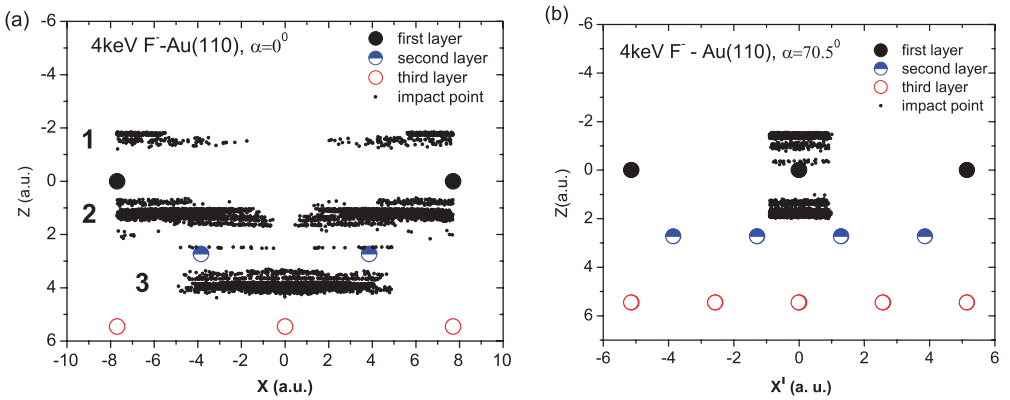

FIG. 8. (Color online) A side view of the Au(110) surface in which the points indicate the apex positions of 4-keV fluorine ion trajectories which reach the detector (a) for 0° and (b) for 70.5° azimuthal angle. The atomic positions of the first layer, second layer, and third layer of the surface are shown in the figures, respectively. The smallest solid points indicate the positions of the impact zones (trajectory apex z) of the ions. Negative z values correspond to regions above the surface. Axis x' in figure (b) is the projection of the x axis at 70.5°.

two typical trajectories and the effective electron densities encountered along the particle's path. In this case the most probable energy losses are more widely set apart and both have quite large contributions.

The most probable energy losses, corresponding to scattering above and below the surface, for the 70.5° direction, are compared in Fig. 5 with the experimental data. As is evident already from the comparison with the shapes of the spectra these positions are correctly reproduced.

A comparison of the most probable energy losses for top scattering in the simulations shows that the energy loss is the largest for the 0° direction (about 65 eV) and lower for the 70.5° and 90° directions (about 57 eV in both cases). The reason for this is qualitatively clear from the drawing of the surface in Fig. 1. For the 0° direction the ions scattering on top of the atomic rows encounter atoms lying closer to each other than seen with scattering directions going above the missing row and thus traverse an effectively higher electron density, leading to larger losses.

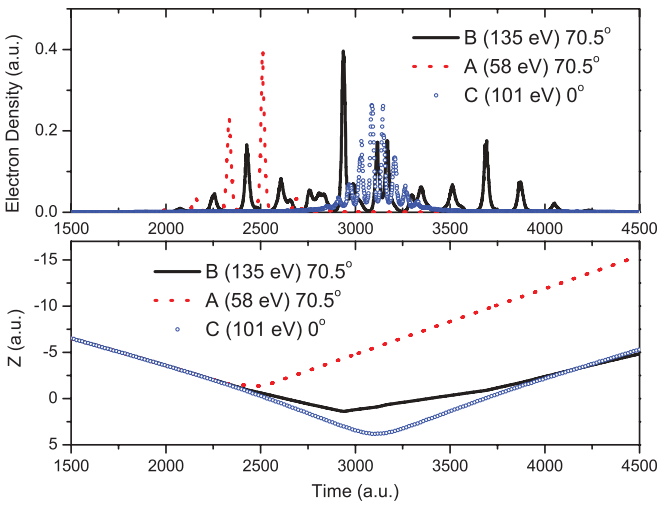

FIG. 9. (Color online) Two characteristic trajectories A and B (z dependence versus time) for 4-keV F^- scattered from Au(110) along the 70.5° direction (bottom panel), corresponding to 58-eV (solid circles) and 135-eV losses (black line) and corresponding to the relevant electron densities "seen" by the projectile (top panel). Also shown is a trajectory C (open circles) for 4 keV scattering along the 0° azimuth exactly in the middle of the missing row and corresponding electron density "seen" by the projectile (open circles). The energy loss in the latter case is 101 eV.

Another feature of the energy-loss spectra is that the energy loss for scattering below the first atomic layer is the greatest for the 70.5° direction (135 eV) than for the 0° and 90° directions (101 and 108 eV, respectively). To analyze this we compare in Fig. 9 the trajectory and the electron density encountered by atoms scattered in the 0° direction exactly in the middle of the channel. The calculated energy loss in this case is 101 eV. For 70.5° the particles encounter a slightly greater number of atomic centers with rather different electron densities as compared to the 0° direction. *A priori* it is not entirely obvious that a larger energy loss should ensue, but the calculation shows that this is in fact the case.

VI. CONCLUSIONS

In conclusion, a joint experimental and theoretical study on scattering of keV fluorine ions scattered off a reconstructed Au(110) single-crystal surface was reported for various azimuthal orientations under grazing scattering conditions. The surviving negative ion fraction was measured as a function of azimuthal angles of the crystal for 3- and 4-keV fluorine ions. The more interesting finding here is the negative ion fraction's azimuth dependence which has not been reported previously on metal surfaces. We did not analyze this in detail here, but it is plausible that this effect is related to the strong corrugation of the electron density above the surface leading to rather different "effective" atom-surface interaction distances akin to the effect of scattering on a stepped surface.

For different azimuthal angles of the crystal, significant changes of energy loss are observed in the measured spectra. In particular, in some cases, as for the 3.6° and 70.5° directions, we observe an evident splitting of the energy-loss spectrum into two components. The most probable energy losses for different azimuthal orientations increase linearly with the increase of incident energies. In order to understand the experimental energy-loss spectra, we use a model developed

previously to analyze the ion trajectory and simulate the energy-loss spectra. This simulation takes into account the correct corrugation of the electron density above the surface and thus allows us to describe the main features in the energy-loss spectra.

The structures in the spectra can be assigned to different classes of trajectories that probe regions of different electron densities and thus lead to different energy losses. One type of the trajectories is from the scattering on the top atoms of the surface, which contributes to the lower energy-loss peak of the energy-loss spectrum; and another one from the in-row scattering is related with the higher energy-loss peak. The relative weights of these trajectories determine the structure of the spectra and are responsible for the splitting into two distinct peaks for some azimuthal angles. Some other finer details of differences of energy losses for different azimuthal orientations could also be described in terms of the model presented.

Overall, this study clearly shows that surface electronic density corrugation is important in describing ion surface scattering processes, which gives correctly the energy-loss distributions for different crystalline directions.

ACKNOWLEDGMENTS

This work was supported by the France-Chile, ECOS-Conicet, and ECOS-Conicyt collaboration projects, FONDECYT (Grant No. 1100759), Grant No. USM-DGIP 11.08.57, Financiamiento Basal para Centros Científicos y Tecnológicos de Excelencia, CEDENNA, CONICYT/Programa Bicentenario de Ciencia y Tecnología (CENAVA) PBCTACT027, and the Millennium Scientific Initiative. The authors gratefully acknowledge useful discussions with N. R. Arista. L. Chen thanks the China Scholarship Council, which made his stay at ISMO (ex Laboratoire des Collisions Atomiques et Moléculaires) possible.

[1] J. Lindhard, *Mat. Fys. Medd. K. Dan. Vidensk. Selsk.* **34**, 14 (1965); D. S. Gemmell, Rev. Mod. Phys. **46**, 129 (1974).
[2] T. L. Alford, L. C. Feldman and J. W. Mayer, *Fundamentals of Nanoscale Film Analysis* (Springer, Berlin, 2007).
[3] C. Rau and R. Sizmann, Phys. Lett. A **43**, 317 (1973).
[4] G. Zampieri, F. Meier, and R. Baragiola, Phys. Rev. A **29**, 116 (1984); S. Lacombe, L. Guillemot, M. Huels, T. Vu Ngoc, and V. A. Esaulov, Surf. Sci. **295**, L1011 (1993); L. Guillemot, S. Lacombe, V. N. Tuan, V. A. Esaulov, E. Sanchez, Y. A. Bandurin, A. I. Dashchenko, and V. G. Drobnich, *ibid.* **365**, 353 (1996).
[5] H. Winter, Phys. Rep. **367**, 387 (2002).
[6] K. Kimura, M. Hasegawa, and M. Mannami, Phys. Rev. B **36**, 7 (1987).
[7] A. Närmann, R. Monreal, P. M. Echenique, F. Flores, W. Heiland, and S. Schubert, Phys. Rev. Lett. **64**, 1601 (1990); H. Winter, C. Auth, A. Mertens, A. Kirste, and M. J. Steiner, Europhys. Lett. **41**, 437 (1998).
[8] Z. Y. Zhao, A. M. Arrale, S. L. Li, D. K. Marble, D. L. Weathers, S. Matteson, J. M. Anthony, B. Gnade, and F. D. McDaniel, Phys. Rev. A **57**, 2742 (1998).
[9] A. Garcia-Lekue and J. M. Pitarke, Phys. Rev. B **64**, 35423 (2001).
[10] M. Alducin, V. M. Silkin, J. I. Juaristi, and E. V. Chulkov, Phys. Rev. A **67**, 032903 (2003).
[11] J. E. Miraglia and M. S. Gravielle, Phys. Rev. A **67**, 062901 (2003).
[12] A. Robin, D. Niemann, N. Stolterfoht, and W. Heiland, Phys. Rev. A **67**, 052901 (2003).
[13] A. Robin, J. Jensen, D. Osterman, and W. Heiland, Nuc. Inst. Methods B **193**, 568 (2002).
[14] A. Niehof and W. Heiland, Nucl. Inst. Methods B **48**, 306 (1990).
[15] A. Närmann, W. Heiland, R. Monreal, F. Flores, and P. M. Echenique, Phys. Rev. B **44**, 1991 (2003).
[16] H. Winter, J. I. Juaristi, I. Nagy, A. Arnau, and P. M. Echenique, Phys. Rev. B **67**, 245401 (2003).
[17] P. M. Echenique and A. Arnau, Phys. Scr. **T49**, 677 (1993).
[18] L. Guillemot, E. Sanchez, and V. A. Esaulov, Nucl. Inst. Methods B **212**, 20 (2003).
[19] J. E. Valdés, C. Parra, J. Díaz-Valdés, C. D. Denton, C. Agurto, F. Ortega, N. R. Arista, and P. Vargas, Phys. Rev. A **68**, 064901 (2003); E. A. Figueroa, E. D. Cantero, J. C. Eckardt, G. H. Lantschner, J. E. Valdés, and N. R. Arista, *ibid* **75**, 010901(R) (2007).
[20] J. E. Valdés, P. Vargas, L. Guillemot, and V. A. Esaulov, Nucl. Inst. and Methods B **256**, 81 (2007); J. E. Valdés, P. Vargas, C. Celedón, E. Sanchez, L. Guillemot, and V. A. Esaulov, Phys. Rev. A **78**, 32902 (2008).
[21] L. Chen, J. E. Valdés, P. Vargas, and V. A. Esaulov, J. Phys. Condens. Matter **22**, 345005 (2010).
[22] D. Valdés, J. M. Blanco, V. A. Esaulov, and R. C. Monreal, Phys. Rev. Lett. **97**, 047601 (2006); Phys. Rev. B **75**, 165404 (2007).
[23] A. G. Borissov and V. A. Esaulov, J. Phys. Condens. Matter **12**, R177 (2000); A. R. Canario, A. G. Borissov, J. P. Gauyacq, and V. A. Esaulov, Phys. Rev. B **71**, 121401 (2005); M. Maazouz, L. Guillemot, and V. A. Esaulov, *ibid.* **15**, 9267 (1997).
[24] M. Maazouz, A. G. Borisov, V. A. Esaulov, J. P. Gauyacq, L. Guillemot, S. Lacombe, and D. Teillet-Billy, Phys. Rev. B **55**, 13869 (1997); L. Guillemot, S. Lacombe, and V. A. Esaulov, Nuc. Inst. Methods B **164**, 601 (2000); S. Ustaze, L. Guillemot, V. A. Esaulov, P. Nordlander, and D. C. Langreth, Surf. Sci. **415**, L1027 (1998).
[25] J. A. Nieminen, Phys. Rev. Lett. **74**, 3856 (1995).
[26] A. Nuber, M. Higashiguchi, F. Forster, P. Blaha, K. Shimada, and F. Reinert, Phys. Rev. B **78**, 195412 (2008).
[27] E. Sanchez, L. Guillemot, and V. A. Esaulov, Phys. Rev. Lett. **83**, 428 (1999).
[28] W. Eckstein, *Computer Simulations of Ion-Solid Interactions* (Springer, Berlin, 1991), Vol. 10.
[29] D. J. O'Connor and J. P. Bierzack, Nuc. Inst. Methods B **15**, 14 (1986).
[30] O. Jones, P. J. Jennings, and O. Jepsen, Phys. Rev. B **29**, 6474 (1984).
[31] N. V. Smith, C. T. Chen, and M. Weinert, Phys. Rev. B **40**, 7565 (1989).